VDMA
Fluid Power Association

22nd ISC

International Sealing Conference

Stuttgart, Germany
October 01 - 02, 2024

Sealing Technology –
Challenges accepted!

UNI STUTTGART

ISBN 978-3-8163-0768-6

Fachverband Fluidtechnik im VDMA e. V. Lyoner Str. 18
50628 Frankfurt am Main
Germany

Phone +49 69 6603-1513
E-Mail maximilian.baxmann@vdma.org
Internet www.vdma.org/fluid

Direct numerical simulation of mixed lubrication in elastohydrodynamic systems

Tim Hantusch, Böðvar Ólafsson, Casper Schousboe Andreasen

The present work proposes a direct numerical model for reciprocating sealing systems which are subject to mixed lubrication. A model is developed to predict tribological characteristics such as friction and leakage in mixed lubrication. The direct implementation allows a seamless coupling between macro-, micro-, and fluid mechanics and ensures full accountability for the highly non-linear material properties. The experimental validation of the model was performed on a newly developed test rig for reciprocating seals where the friction force was measured and compared to the friction force obtained by numerical analysis. The model can be used for the simulation of rod as well as piston seals.

1 Introduction

In the field of hydraulics, reciprocating rod and piston seals are crucial for the performance of cylinders and actuators. With respect to energy efficiency, leakage as well as product lifetime, numerical design tools play an important role in the design process of these seals. Early studies of the elastohydrodynamic lubrication (EHL) theory date back to the 1970's [1], [2] with later application for line contacts [3], [4] and reciprocating seals [5]. Contact mechanics models as the ones proposed by [6] and [7] along with technological progress in computing made it possible to couple solid, micro, and fluid mechanics and hence to build numerical models for mixed lubrication regimes. The obtained coupled equations can be solved both inverse and direct. The inverse method requires that the hydrodynamic pressure distribution is known to calculate the film thickness. Common models for mixed lubrication that use the inverse method use commercial FEA software to compute the static contact pressure and export an influence coefficient matrix to find the transient equilibrium in a custom offline program [8], [9], [10]. Direct methods on the other hand solve the Reynolds equation by discretizing the domain, forming a system of algebraic equations, and directly solving these to obtain the pressure distribution. Hence, direct methods require less initial knowledge about the fluid pressure distribution and include deformation of the sealing lip due to deviations between static and hydrodynamic pressure. The direct method has been used to solve mixed elastohydrodynamic lubrication for axisymmetric O-rings by [11] and [12] . Based on this work and inspired by [13], a 2-component sealing system was studied in the presented work. The model was exclusively implemented within the COMSOL® Multiphysics platform and hence allows a full coupling between macro-, micro- as well as fluid mechanics.

The validation of the numerical model is done using a test rig for friction caused by reciprocating seals. The surface of the sealing lip is characterized by 3D surface texture measurement. Finally, the coefficient of friction for the rod-seal contact pair is determined using an application-oriented test apparatus. The purpose of this work is to apply and validate the direct method for a multi-part elastohydrodynamic system. Focus is put on a profound experimental study which, along with the numerical results, provides insights into the accuracy of directly solved mixed lubrication models.

2 Numerical model

A sealing system consisting of an O-ring and a PTFE (Polytetrafluorethylene) lip seal is investigated. This specific sealing system was numerically studied by [14] and [15] using the inverse method. The system is shown in Figure 1. The rod is considered smooth whereas the surface roughness of the seal needs to be taken in to account. The simulation is carried out using 2D-axisymmetry conditions.

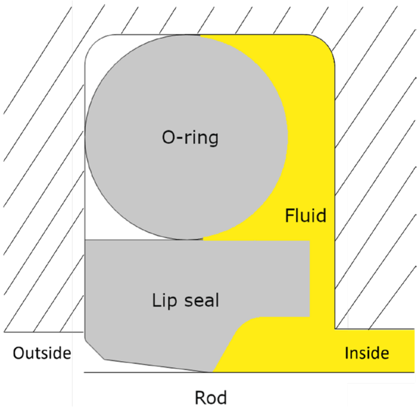

Figure 1: Sealing system

To predict the mechanical response of the O-ring, the hyperelastic Mooney-Rivlin model [16] is utilized. This model describes the strain-energy density as a linear combination of two invariants and two coefficients as seen in (1). The last term in this model describes the volumetric response of the material and can be neglected when assuming incompressibility of the material.

$$W = C_{10}(I_1 - 3) + C_{01}(I_2 - 3) + D_1(J - 1)^2 \tag{1}$$

The material used is bronze-filled PTFE which is modelled using a non-linear elastic material model calibrated with compression test data according to ISO 604 [17].

To solve the fluid mechanics in the gap between rod and seal, the Reynolds equation is used. Side leakage is neglected as axisymmetric conditions apply. Moreover, the fluid is assumed to be Newtonian and incompressible. Under these assumptions the Reynolds equation for the investigated problem takes the form:

$$\frac{\partial}{\partial x}\left(\frac{h^3}{\eta}\frac{\partial p_f}{\partial x}\right) = 12\overline{u}\frac{\partial h}{\partial x} \tag{2}$$

With respect to the finite-element implementation, the Reynolds equation is stated in its weak form:

$$\int_{\Omega}\left[\nabla\delta p_f \cdot \left(\frac{h^3}{12\eta}\nabla p_f\right) + \delta p_f \nabla(\overline{u}h)\right] d\Omega = 0 \tag{3}$$

The above equation requires the implementation of boundary conditions. In this case, Dirichlet boundary conditions are chosen and yield:

$$p_f(x = x_0) = p_{system}\ ;\ p_f(x = x_{max}) = p_{atm} \tag{4}$$

As the total load consists of a hydrodynamic and an asperity component, the friction force is the sum of the hydrodynamic shear force and the shear force caused by interacting asperities over the contact area and hence can be written as:

$$F_{f,tot} = \int_{A_{con}} \left(\tau_{asp} + \tau_f\right) dA \tag{5}$$

In terms of finite-element implementation, the total friction force takes the following form:

$$F_{f,tot} = \sum_{i=1}^{N} \int_{\Omega_i} \left(\mu p_{asp} + \frac{2\eta\overline{u}}{h}\right) d\Omega \tag{6}$$

To determine the coefficient of friction caused by the asperities a statistical model is used. The coefficient of friction for a single asperity is defined as the ratio between shear stress and pressure and is given in (7).

$$\mu_i = \frac{\tau_{asp,i}}{p_{asp,i}} \tag{7}$$

[6] proposed a widely used model to determine the asperity contact pressure, p_{asp}, in which they considered a nominally flat surface which is covered with asperities of identical radius β. The asperity height on the other hand varies randomly. Using a reference plane in the rough surface, [6] describe the probability that a particular asperity has a height between z and $z + dz$ as $\phi(z)dz$. Hence, the probability that an asperity has a height greater than the separation h can be written as shown in (8).

$$prob(\mathrm{z} > h) = \int_{h}^{\infty} \phi\,(z)dz \tag{8}$$

Thus, the total area of contact is defined as stated in (9).

$$A = \pi N\beta \int_{h}^{\infty} (z - h)\, \phi(z) dz \tag{9}$$

Finally, the total load is given in (10).

$$P = \frac{4}{3} N E' \beta^{1/2} \int_{h}^{\infty} (z - h)^{3/2}\, \phi(z) dz \tag{10}$$

Assuming that the distribution of asperity heights is Gaussian, (11) can be used for the probability function.

$$\phi * (s) = \frac{1}{\sqrt{2\pi}} e^{-\frac{s^2}{2}} \tag{11}$$

Combining (9), (10) and (11) the following expression for the asperity contact pressure is obtained:

$$p_{asp} = \frac{4}{3} E' n \beta^{1/2} \sigma^{3/2} \frac{1}{\sqrt{2\pi}} \int_{h_n}^{\infty} (s - h_n)^{3/2}\, e^{-\frac{s^2}{2}} ds \tag{12}$$

A solution for the elastohydrodynamic problem with mixed lubrication must therefore satisfy the equilibrium shown in (13).

$$p_c = p_f + p_{asp} \tag{13}$$

For the direct numerical model presented in this paper, the static FEA model of the sealing system was extended by (3) as a weak form boundary PDE. Since (12) is a statistical expression, it could not be assigned into a weak form. Hence, the surface mechanics model was added as an analytical expression. The statistical character of the Greenwood-Williamson model makes it difficult to solve for as FEA deals with deterministic problems where explicit boundary conditions can be stated. [18] has therefore suggested to perform a curve fit to obtain an analytically invertible expression for the film thickness. In this work, it was found that the statistical expression as suggested by [6] could be solved within a reasonable amount of time assuming proper scaling of variables as well as fine-tuned solver settings. The mesh size at the lip-rod interface is set to $2\mu m$ with a curvature factor of 0.01 to ensure accurate results. For the same reason, the contact model at this interface, which includes friction, is of augmented Lagrangian type. The shape functions used for both solid and fluid mechanics in this model are quadratic Lagrangian.

The scheme of the model is illustrated in Figure 2. The provided input data includes geometric properties of the sealing system, surface parameters, structural and tribological material properties as well as the application parameters. The proposed model follows the loading sequence which the sealing system would undergo under real conditions. First, the seal is mounted. Next, pressure is applied while the system remains static. In further progress of the simulation, the static contact pressure is calculated using the surface mechanics model. Finally, motion is applied to the rod and the transient system consisting of structural mechanics, surface mechanics and fluid mechanics is directly solved. The output includes the transient asperity pressure, the transient fluid pressure, the friction force, and the leakage.

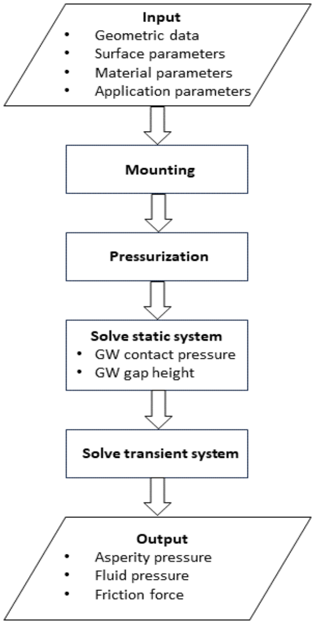

Figure 2: Multi-step numerical model

3 Identification of material parameters

As this work aims to validate the proposed numerical model by experimental investigation, an accurate determination of material parameters used in the equations presented in chapter 2 is required.

To start with, the Greenwood-Williamson surface model requires a profound investigation of the surface texture to determine the parameters σ, β and n. For this project a 3D surface texture measurement is performed using a high-resolution optical instrument. Both the values for cut-off length and magnification can be found in Table 1. The profile is evaluated in the transverse direction, i.e. in the direction of the tool during manufacturing. Moreover, the profile is levelled before extraction of surface parameters.

(6) contains the dry coefficient of friction (dry COF) for the contact between sealing lip and piston rod. As the asperity friction force is proportional to the dry COF, it is

important to determine this parameter highly accurate. To do so, a test apparatus as shown in Figure 3 was built for this project. The dry COF is measured from specimens that are cut from the investigated seal and mounted on a load sledge that slides on two parallel piston rods similar to the one mounted in the test rig.

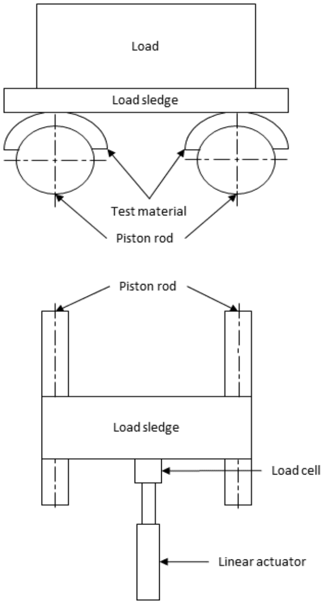

Figure 3: Test setup for the determination of the dry COF

Several studies have shown that the dry COF depends on both the normal load and the sliding velocity [19], [20], [21]. For the determination of the dry COF in this work, a fixed normal load is chosen. The value of this load can be found in Table 1 and is chosen so that approximately half of the area under the contact pressure curve for 100bar in Figure 4 lie below the dry COF test pressure.

Table 1: Material and processing parameters

Parameter	Unit	Value
β	mm	3×10^{-3}
λ_c	mm	25×10^{-3}
μ	$-$	0.085
σ	mm	2×10^{-3}
M	$-$	20
n	$\frac{1}{mm^2}$	1×10^{5}
p_{cof}	MPa	20

4 Numerical results

Here, the results for the operating conditions defined in Table 2 are presented. The static pressure distributions for the investigated pressures are given in Figure 4. The coordinate, which is to be found on the x-axis of the plot, refers to the spatial coordinate of the nodes. The oil is located at the lower coordinate values outside the contact area. This applies for all the figures in this chapter.

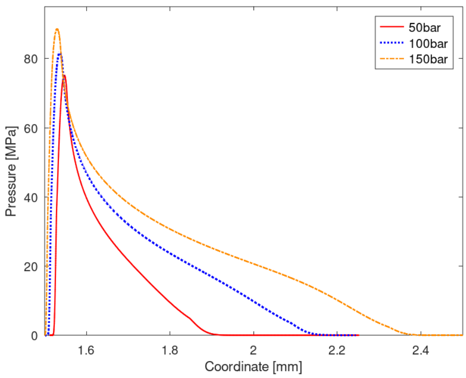

Figure 4: Static contact pressure distribution

Next, the pressure distributions for the outstroke can be seen in Figure 5. Due to the relative motion between rod and seal, the static contact pressure is split up into asperity pressure and fluid pressure fractions.

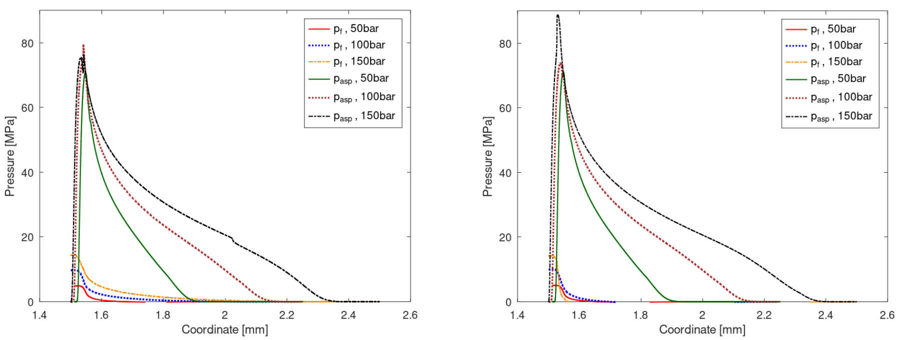

Figure 5: Pressure distributions for 50mm/s (left) and 150mm/s (right), outstroke

For the investigated system, the asperity pressure is significantly higher than the fluid pressure. Towards the air side, the fluid pressure drops to zero. Both investigated velocities show similar pressure distributions. However, the fluid pressure extends further towards the air side for 50 mm/s than for 150 mm/s. For instroke, it is to be noted that the simulation assumes a sufficient amount of oil on the rod in order to properly lubricate the contact zone. Looking at the results in Figure 6, the asperity pressure is found to carry the major share of the total load. At lower pressures up to 100 bar, the pressure distributions are close to the ones obtained for outstroke. For 150bar, the fluid pressure extends significantly longer towards the air side. This applies to both 50 mm/s and 150 mm/s rod velocity.

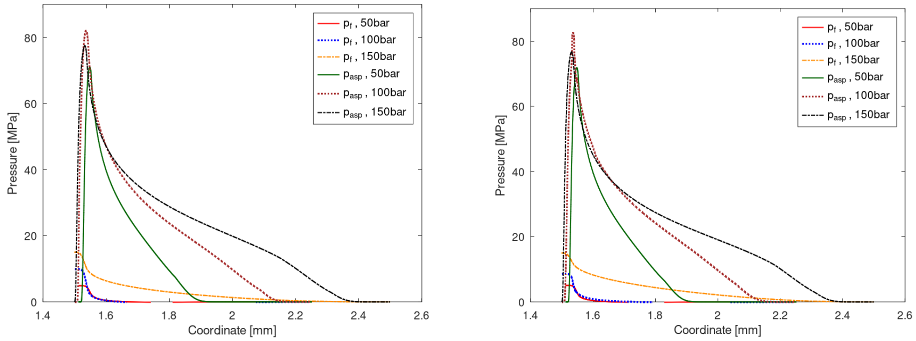

Figure 6: Pressure distributions for 50mm/s (left) and 150mm/s (right), instroke

Figure 7 shows the film thickness for both the static condition as well as instroke and outstroke at 50bar and 100bar respectively. The corresponding film thickness at 150bar is given in Figure 8. For better visualization, the plot contains a zoom-in of the region between maximum and minimum contact pressure gradient.

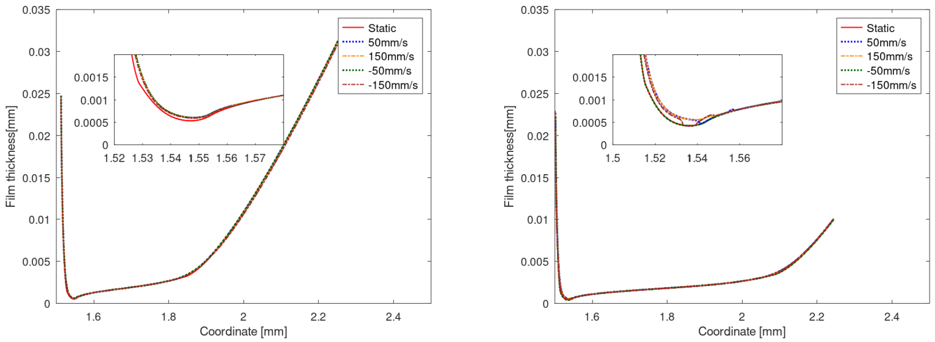

Figure 7: Film thickness for 50bar (left) and 100bar (right)

The deviation between the static and transient film thickness is due to the fluid film pressure and thus dependent on the rod velocity (see chapter 2). Within the analysed velocity range, this dependency cannot be clearly observed for 50bar pressure.

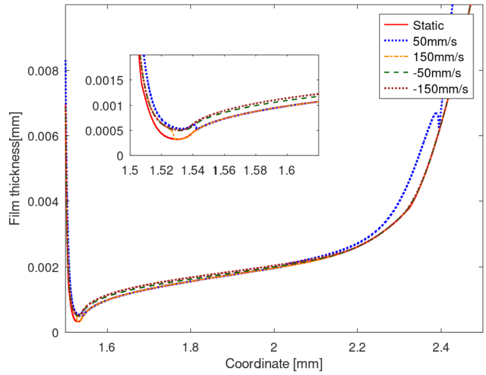

Figure 8: Film thickness at 150bar

5 Experimental setup

To validate the proposed numerical model, a hydraulic test rig for reciprocating seals was developed at *Haagensen A/S*. The test rig is capable of friction and leakage measurement for both rod and piston seals. Figure 9 shows a simplified sketch of the test rig which consists of a test and a load cylinder, a hydraulic pump station as well as a sensor and control system. The seal to be investigated is mounted in the test cylinder where all other friction sources are eliminated. Both pressure and temperature are constantly measured in the test cylinder. The force transmitted between test and load cylinder is measured by a force transducer and compared to the force acting on either rod or piston in the test cylinder.

Table 2: Test parameters

Parameter	Unit	Value
Rod diameter	mm	40
Fluid	–	Hydraulic oil ISO VG 46
Stroke length	mm	800
Evaluation length	mm	500
Pressure	MPa	50, 100, 150
Rod velocity	$\frac{mm}{s}$	-150, -50, 50, 150
Ambient temperature	°C	23

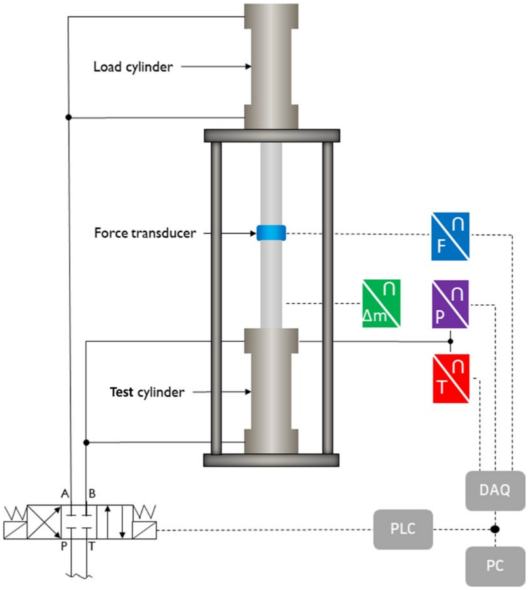

Figure 9: Reciprocating test rig

Test rigs for reciprocating seals can follow different design principles. One commonly used principle uses a symmetric pressurized housing where the piston rod sticks out on both sides of the housing. The advantage of this principle is that the net force on the rod is zero. However, as the housing is symmetric, two seals are needed where always one seal operates on instroke while the other seal is on outstroke. Examples of this test rig can be seen in [22] and [10] . Another principle is the one used in the presented work, where two hydraulic cylinders work against each other. The forces in the cylinder are higher, which requires an accurate measurement of both the cylinder pressure and the transmitted force. Through careful alignment of piston rods of the test and load cylinder, the developed test rig can temporarily run without additional guide rings or bushings, ensuring that the investigated seal is the only source of friction during the test.

6 Comparison between numerical and experimental results

To validate the proposed numerical model, the friction forces obtained by both simulation and experiment are compared. The results are given in Figure 10. The results for the experimental friction force plotted in this figure are obtained by averaging the friction force over the evaluation length of the stroke, which is defined as the part of the cycle where the rod velocity is at steady state. For each operation point, a total of 7 strokes are evaluated. The results for each evaluated stroke are included in Figure 10, which also contains the simulation results for 10, 20, 30, 40 and 75bar.

The experimental results for instroke match closely with the simulations. At 50bar and 50mm/s, the experiments show a maximum deviation of -5.8% compared to the numerical results. This deviation increases towards higher velocities, resulting in a maximum deviation of +15% for 50bar at 150mm/s. For 150bar, the experiments show a maximum deviation of -13.6% to the numerical results at 50mm/s and a maximum deviation of -11.5% at 150bar.

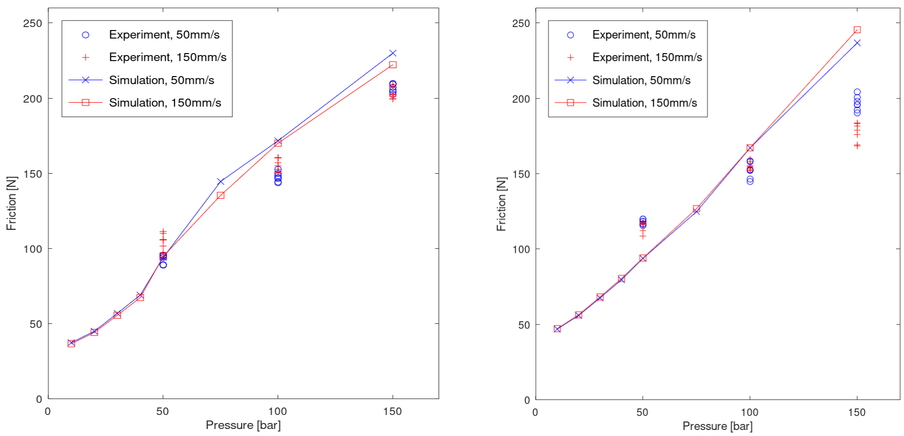

Figure 10: Instroke(left) and outstroke (right) friction force

The deviations for outstroke are in general slightly higher than the ones seen for instroke. At 50bar and 50mm/s, the experiments show a maximum deviation of +27.5% compared to the numerical results. At 150bar and 150mm/s, this maximum deviation is found to be -31%.

Although there is a good overall agreement between experiments and simulations, the simulations tend to underestimate the friction force for low pressures. This is concluded based on the results obtained at 50bar pressure for both test velocities on in- and outstroke. At higher pressures, the simulations overestimate the friction force for both test velocities on in- and outstroke. A possible explanation for the increasing overestimation of the friction force towards higher pressures could be found in chapter 3, where it is stated that the friction coefficient for PTFE is load dependent and decreases with increasing load [19], [20], [21] .

7 Conclusion

The presented work introduces a direct numerical model for reciprocating sealing systems which are subject to mixed lubrication. The implementation of the model is done exclusively within the COMSOL® Multiphysics platform. The numerical model covers solid mechanics, surface mechanics as well as fluid mechanics by manual implementation of the Reynolds equation as a weak boundary PDE and the Greenwood-Williamson surface model as an analytical expression. The full coupling between macro-, micro- and fluid mechanics allows for a continuous adjustment of non-linear material properties and a deviation between static and dynamic contact pressure. The model is characterized by a high robustness as well as a short set-up time. Provided a profound analysis of the seal's surface texture and an application-oriented determination of the friction coefficient, the model shows good agreement with experimentally obtained data for the friction force for both instroke and outstroke motion of the rod. For instroke, the accuracy of simulation results is closer to the experimental values than for outstroke.

The results presented in this paper show that complex tribological models can be implemented within a single multiphysics platform while reaching a high agreement with experimentally obtained data. This way, set-up and computation time can be reduced significantly. Using correct values for the friction coefficient and the surface texture parameters is crucial for an accurate determination of the fluid film thickness and friction force in mixed lubrication.

8 Nomenclature

Variable	***Description***	***Unit***
Ω	Domain indicator	$[-]$
β	Radius of asperities	$[mm]$
δ	Laplace operator	$[-]$
η	Dynamic viscosity	$[MPas]$
λ_c	Cut-off length	$[mm]$
μ	Friction coefficient	$[-]$
σ	Standard deviation of peak heights	$[mm]$
τ_{asp}	Asperity shear stress	$[MPa]$
τ_{f}	Viscous shear stress	$[MPa]$
∇	Gradient operator	$[-]$
A_{con}	Contact area	$[mm^2]$
C_{ij}	Material model parameter(s)	$[MPa]$
D_i	Volumetric response parameter(s)	$[MPa]$
E'	Effective Young's modulus	$[MPa]$
$F_{f,tot}$	Total friction force	$[N]$
I_i	Matrix invariant(s)	$[-]$
J	Determinant of deformation gradient	$[-]$
M	Magnification factor	$[-]$
N	Number of asperities	$[-]$
W	Strain energy density	$[MPa]$
$\overline{u}$	Mean velocity, $\frac{u_a+u_b}{2}$	$[\frac{mm}{s}]$

h	Film thickness	$[mm]$
h_n	Standardized film thickness, $\frac{h}{\sigma}$	$[-]$
n	Asperity density	$[\frac{1}{mm^2}]$
p_{asp}	Asperity pressure	$[MPa]$
p_{cof}	Pressure for determination of μ	$[MPa]$
p_c	Contact pressure	$[MPa]$
p_f	Fluid pressure	$[MPa]$
x	Coordinate variable	$[mm]$

9 References

[1] B. J. Hamrock and D. Dowson, “Isothermal Elastohydrodynamic Lubrication of Point Contacts: Part II—Ellipticity Parameter Results,” *Journal of Lubrication Technology*, vol. 98, no. 3, pp. 375–381, Jul. 1976, doi: 10.1115/1.3452861.

[2] B. J. Hamrock and D. Dowson, “Isothermal Elastohydrodynamic Lubrication of Point Contacts: Part 1—Theoretical Formulation,” *Journal of Lubrication Technology*, vol. 98, no. 2, pp. 223–228, Apr. 1976, doi: 10.1115/1.3452801.

[3] B. J. Hamrock and J. H. Tripp, “Numerical methods and computers used in elastohydrodynamic lubrication,” in *Developments in Numerical and Experimental Methods Applied to Tribology*, Elsevier, 1984, pp. 11–19. doi: 10.1016/B978-0-408-22164-1.50005-3.

[4] M. K. Ghosh and B. J. Hamrock, “Thermal Elastohydrodynamic Lubrication of Line Contacts,” *A S L E Transactions*, vol. 28, no. 2, pp. 159–171, Jan. 1985, doi: 10.1080/05698198508981608.

[5] A. F. C. Kanters, “Paper XIII (i) On the Elastohydrodynamic Lubrication of Reciprocating Elastomeric Seals: The Influence of the Surface Roughness,” 1991, pp. 357–364. doi: 10.1016/S0167-8922(08)70152-4.

[6] J. A. Greenwood and J. B. P. Williamson, “Contact of Nominally Flat Surfaces,” 1966. [Online]. Available: https://about.jstor.org/terms

[7] A. W. Bush, R. D. Gibson, and T. R. Thomas, “The elastic contact of a rough surface,” *Wear*, vol. 35, no. 1, pp. 87–111, Nov. 1975, doi: 10.1016/0043-1648(75)90145-3.

[8] R. F. Salant, N. Maser, and B. Yang, “Numerical model of a reciprocating hydraulic rod seal,” *J Tribol*, vol. 129, no. 1, pp. 91–97, Jan. 2007, doi: 10.1115/1.2401222.

[9] A. K. Bullock, D. G. Tilley, D. N. Johnston, C. R. Bowen, and P. S. Keogh, “Non-linear friction in reciprocating hydraulic rod seals: Simulation and measurement,” in *Journal of Physics: Conference Series*, Institute of Physics Publishing, 2009. doi: 10.1088/1742-6596/181/1/012009.

[10] C. Xiang, Z. Wang, X. Jia, and F. Guo, “Numerical simulation model of a reciprocating seal based on the mixed-lubrication theory,” *The Journal of Engineering*, vol. 2019, no. 13, pp. 49–53, Jan. 2019, doi: 10.1049/joe.2018.8948.

[11] T. Schmidt, M. André, and G. Poll, “A transient 2D-finite-element approach for the simulation of mixed lubrication effects of reciprocating hydraulic rod seals,” *Tribol Int*, vol. 43, no. 10, pp. 1775–1785, Oct. 2010, doi: 10.1016/j.triboint.2009.11.012.

[12] S. Stupkiewicz, “Finite element treatment of soft elastohydrodynamic lubrication problems in the finite deformation regime.”

[13] T. Lohner, A. Ziegltrum, J. P. Stemplinger, and K. Stahl, “Engineering Software Solution for Thermal Elastohydrodynamic Lubrication Using Multiphysics Software,” *Advances in Tribology*, vol. 2016, 2016, doi: 10.1155/2016/6507203.

[14] H. Ran, S. Wang, and D. Liu, “A multiscale wear model for reciprocating rod stepseal under mixed lubricating conditions based on linear elasticity,” *Proceedings of the Institution of Mechanical Engineers, Part J: Journal of Engineering Tribology*, vol. 235, no. 1, pp. 161–180, Jan. 2021, doi: 10.1177/1350650120902602.

[15] R. F. Salant, B. Yang, and G. W. Woodruff, “NUMERICAL MODELING OF RECIPROCATING FLUID POWER SEALS,” 2008.

[16] “Large elastic deformations of isotropic materials. I. Fundamental concepts,” *Philosophical Transactions of the Royal Society of London. Series A, Mathematical and Physical Sciences*, vol. 240, no. 822, pp. 459–490, Jan. 1948, doi: 10.1098/rsta.1948.0002.

[17] ISO, “ISO 604:2002; Plastics - determination of compressive properties,” 2002.

[18] J. L. Streator and G. W. Woodruff, “A Model of Mixed Lubrication with Capillary Effects.”

[19] T. T. Tevruz¨, “Tribological behaviours of bronze-filled polytetrafluoroethylene dry journal bearings,” 1999.

[20] M. A. Chowdhury *et al.*, “Frictional Behavior of Polymers Sliding Against Smooth and Rough Mild Steel Counter Faces,” *Middle-East Journal of Scientific Research*, vol. 21, no. 3, pp. 477–486, 2014, doi: 10.5829/idosi.mejsr.2014.21.03.21161.

[21] H. Unal, “Tribological Studies of Bronze Filled PTFE Polymer.”

[22] O. Heipl and H. Murrenhoff, “Friction of hydraulic rod seals at high velocities,” *Tribol Int*, vol. 85, pp. 66–73, 2015, doi: 10.1016/j.triboint.2015.01.002.

10 Authors

Haagensen A/S, Hejrevang 6, 3450 Allerød, Denmark:
Tim Hantusch, R&D Engineer, M.Sc., tih@haagensenseals.com

Technical University of Denmark (DTU), Department of Civil and Mechanical Engineering, Section of Solid Mechanics
Koppels Allé, Building 404, 2800 Kongens Lyngby, Denmark
Böðvar Ólafsson, Mechanical Engineer, M.Sc.

Technical University of Denmark (DTU), Department of Civil and Mechanical Engineering, Section of Solid Mechanics
Koppels Allé, Building 404, 2800 Kongens Lyngby, Denmark
Casper Schousboe Andreasen, Associate Professor, PhD, csan@dtu.dk

https://doi.org/10.61319/NPEWSCWX